Electronic Supplementary Material (ESI) for Analyst.

Optical absorption and dichroism of single melanin nanoparticles - Supporting information

David Regan,[1,*] Alexandra Mavridi-Printezi,[2] Lukas Payne,[1,3]
Marco Montalti,[2] Paola Borri,[1] and Wolfgang Langbein[3]

[1]*School of Biosciences, Cardiff University, Museum Avenue, Cardiff C F10 3 AX, UK*

[2]*Department of Chemistry, University of Bologna, Via Selmi, 2, 40126 Bologna BO, Italy*

[3]*School of Physics and Astronomy, Cardiff University, The Parade, Cardiff C F24 3 AA, UK*

(Dated: June 18, 2023)

CONTENTS

* ReganDC@cardiff.ac.uk

S1. NANOPARTICLE SYNTHESIS

All reagents, solvents and chemicals were purchased from Sigma-Aldrich and used without modification, unless otherwise stated.

S1i. Polydopamine Nanoparticles

Polydopamine (PDA) melanin was prepared by the spontaneous oxidation of dopamine hydrochloride in aerobic and alkaline conditions[1]. Initially, 40 ml of ethanol and 90 ml deionised water were mixed in a 250 ml round bottom flask. To the flask was added 2 ml of 28-30% NH_4OH and the mixture was stirred vigorously for 10 min. Next, a dopamine hydrochloride solution was prepared by solubilising 400 mg of dopamine hydrochloride in 10 ml deionised water. The dopamine solution was quickly injected into the flask under vigorous stirring. An immediate colour change was observed, which evolved in time from light yellow to dark brown. The reaction was carried out for 24 hours under vigorous stirring. The NPs were subsequently retrieved by centrifugation at a relative centrifugal force (RCF) of 18,293 g for 20 min. Then, they were washed with deionised water three times at 9333 g and re-dispersed in water.

S1ii. L-DOPA Nanoparticles

In a 100 ml round bottom flask, 70 mg of L-DOPA was dissolved by stirring in 50 ml of water heated to 55-60°C, yielding a 7 mM solution [2] After solubilisation, the solution was allowed cool to room temperature before 360 µl of 1 M $KMnO_4$ solution was added to the round bottom flask to initiate polymerisation. The solution was subjected to vigorous stirring for 24 hours during which the colour of the solution initially changed to red, then gradually to dark brown. The NPs were subsequently retrieved by centrifugation at 9333 g and were washed three times with deionised water, centrifuging them at the same speed and redispersing them in water. To remove the Mn^{2+} ions present, HCl solution (10 ml of 0.1 M) was slowly added to the NPs; the acidification was repeated twice, centrifuging each time at 9333 g. Finally the pellets were washed once more with water and were redispersed.

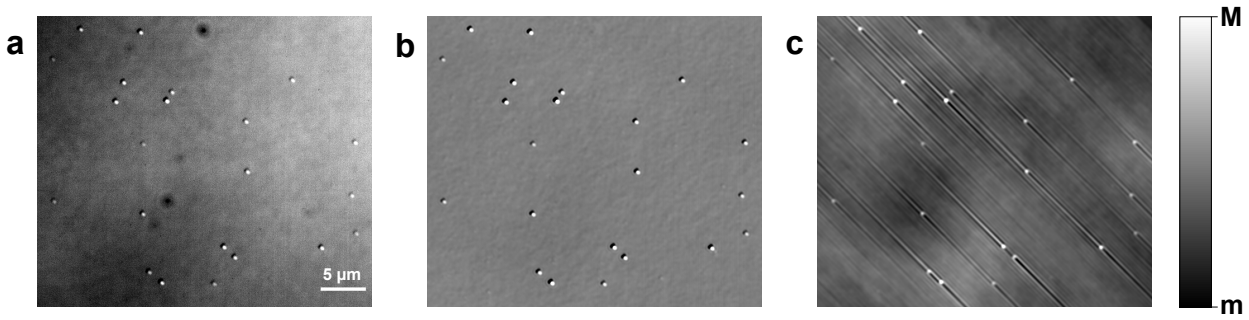

FIG. S1. a) One of the two raw DIC images, taken with a polariser angle of 30° (m = 48000 counts, M = 53000 counts). b) qDIC delta image produced by combining the raw DIC image in a) with one taken at the opposite polariser angle (m = -0.02 rad, M = 0.02 rad). c) qDIC phase image produced by a Wiener deconvolution based integration of the image in b) with a signal to noise parameter of 1000 (m = -0.02 rad, M = 0.04 rad).

S1iii. Sepia Nanoparticles

Sepia melanin was extracted from the ink sac of a cuttlefish (*Sepia officinalis*) and was diluted in distilled water. The NPs were retrieved by centrifugation at a RCF of 2823 g for 10 min and were washed at the same RCF three times with distilled water. After washing, the NPs were redispersed in distilled water.

S2. QUANTITATIVE DIC

As described in our previous work [3], we use quantitative DIC (qDIC) to characterise the NPs. qDIC reconstructs a quantitative phase profile of a sample from two standard DIC images taken at opposite phase offsets using Wiener filtering. The qDIC process is illustrated in Fig. S1a-c, which compares a raw DIC image in a) (taken at one of the two polariser angles used) with a δ image in b) (the retrieved phase difference in radians) and a quantitative phase image in c) derived from the δ image by the Wiener filter. Elongated artefacts in the image along the DIC shear originate from the integration with missing gradient information perpendicular to the DIC shear direction. The extension of these artefacts increases with the signal-to-noise parameter used in the Wiener filter[3], which can be chosen to get accurate results from the analysis. Here, we use a value of 1000.

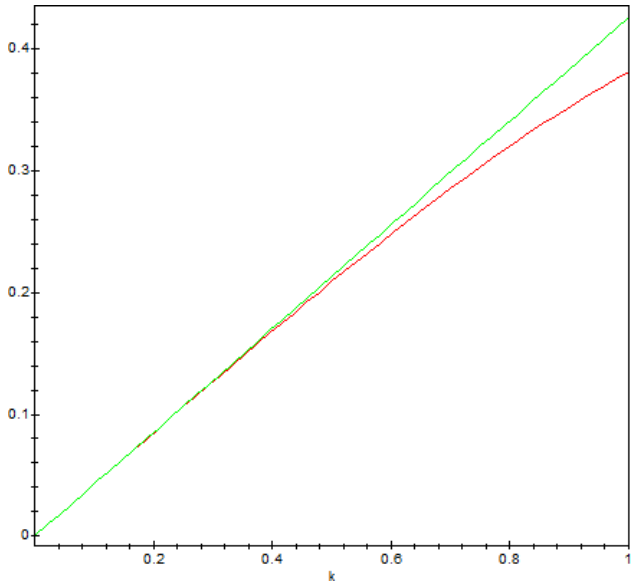

FIG. S2. Factor $\mathrm{Im}\left[(\epsilon_\mathrm{p}-\epsilon_\mathrm{m})/(\epsilon_\mathrm{p}+2\epsilon_\mathrm{m})\right]$ in the absorption cross section Eq. 16 as function of the absorption index κ for $\epsilon_\mathrm{m}=1$ and $n=1.7$ corresponding to the experimental data. Comparison of the full expression (red) and the linear approximation (green) according to Eq. S1.

S3. DETERMINATION OF COMPLEX REFRACTIVE INDEX AND ASPECT RATIO

The determination of the complex refractive index values from the radius and extinction values was handled numerically, by varying the absorption index, κ, for each particle to match the radius calculated using Eq. 16 to the radius calculated from the qDIC phase measurements. We note that for weak absorption, $\kappa \ll 1$, which is the case for melanin in the investigated spectral range, the absorption cross section is approximately proportional to κ, as can be seen by the Taylor development of the imaginary part factor in Eq. 16 around $\kappa = 0$, given by

$$\mathrm{Im}\left[\frac{\epsilon_\mathrm{p}-\epsilon_\mathrm{m}}{\epsilon_\mathrm{p}+2\epsilon_\mathrm{m}}\right] = \frac{6\epsilon_\mathrm{m} n}{(n^2+2\epsilon_\mathrm{m})^2}\kappa + \frac{12\epsilon_\mathrm{m} n(2\epsilon_\mathrm{m}-n^2)}{(n^2+2\epsilon_\mathrm{m})^4}\kappa^3 + \mathcal{O}\left(\kappa^5\right) . \tag{S1}$$

This is exemplified in Fig. S2 using the values $\epsilon_\mathrm{m}=1$ and $n=1.7$ corresponding to the experimental data of melanin NPs in air. Note that $\epsilon_\mathrm{p}=(n+i\kappa)^2$.

The determination of the aspect ratio, b/a, for each particle was handled in a similar way, varying b/a and matching the calculated relative amplitude parameter, α, to the measured value for each particle. For this, the individual absorption index value of each particle

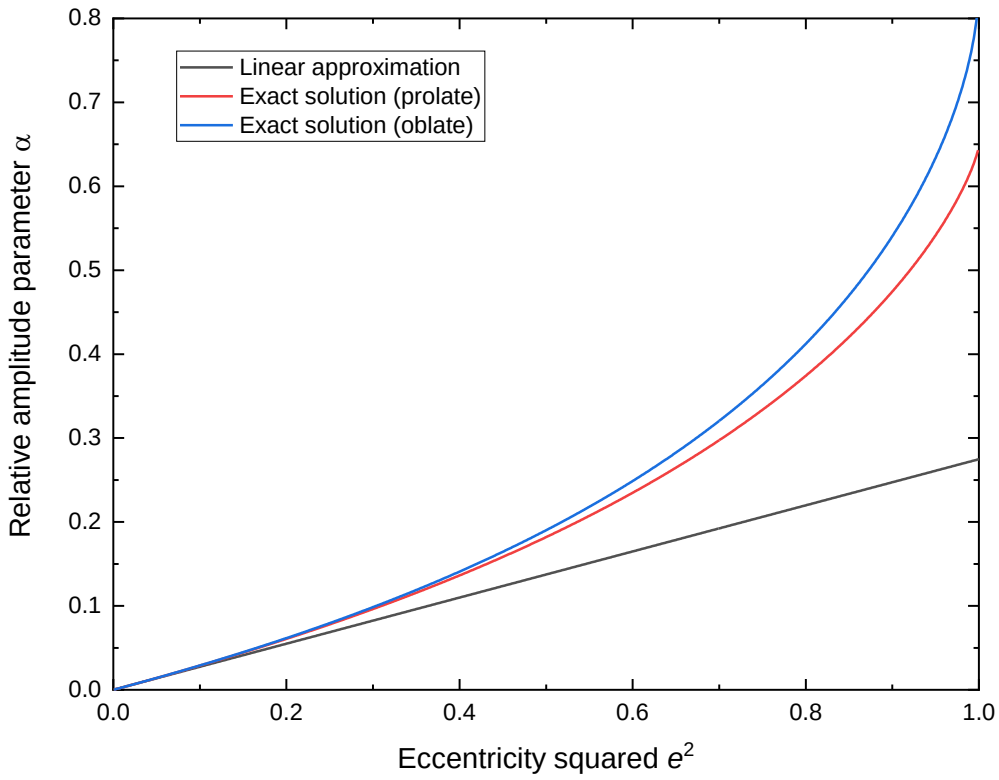

FIG. S3. A plot comparing the linear approximation of α with the exact solution as a function of the eccentricity squared e^2 for L-DOPA nanoparticles at 405 nm.

was used. We note that for small values of the squared eccentricity ($e^2 \ll 1$), α can be approximated by

$$\alpha = \frac{3}{5}\frac{|\epsilon_\mathrm{p}|^2 + \epsilon_\mathrm{m}(\mathrm{Re}(\epsilon_\mathrm{p}) - 2\epsilon_\mathrm{m})}{|\epsilon_\mathrm{p} + 2\epsilon_\mathrm{m}|^2} e^2 \,, \tag{S2}$$

linear in e^2. The comparison between this linear approximation and the full expression is plotted in Fig. S3, using the complex index of L-3,4-dihydroxyphenylalanine (L-DOPA) particles at 405 nm. For particles with $e^2 < 0.21$, the approximation has a relative error below 10%.

Up to now we have assumed prolate particles with axes $a > b = c$, which have a short axis normal to the surface. For oblate particles with $a = c > b$, the geometric factors are [29]

$$L_\mathrm{a} = \frac{\sqrt{e^{-2}-1}}{2e^2}\left(\frac{\pi}{2} - \arctan\left(\sqrt{e^{-2}-1}\right)\right) - \frac{e^{-2}-1}{2}\,, \quad L_\mathrm{b} = 1 - 2L_\mathrm{a}\,. \tag{S3}$$

Such particles have one of the two long axes normal to the surface, which seems less likely to occur as it would reduce the contact surface compared to having the short axis normal to the surface. Non-withstanding this observation, we find that in first order in e^2, we

have $L_a = 1/3 - e^2/15$ and $L_b = 1/3 + 2e^2/15$. For the prolate particles instead, we have $L_a = 1/3 - 2e^2/15$ and $L_b = 1/3 + e^2/15$, which is equal to the oblate case except a swap of axes naming. Therefore, the linear approximation Eq. S2 holds for both prolate and oblate particles, and differences in the retrieved α are only relevant for large e^2.

S4. CALCULATION OF DICHROIC PARAMETERS

As discussed in the main text, the dichroic relative amplitude parameter, α^d, and the dichroic particle orientation, γ^d, are related to the corresponding measured parameters, α^c and γ^c, according to Eq. 14 and Eq. 15. These equations assume that the geometric amplitude parameter, α^g, is constant across all wavelengths. The change in α^g with wavelength can be calculated for a given particle with known eccentricity using Eq. 10, and for a particle with an eccentricity comparable to the measured values over the wavelength range used, α^g changes by an amount more than an order of magnitude smaller than the mean changes in measured α with wavelength, and so is considered negligible in the analysis.

In the absence of a simple analytical solution for α^d and γ^d, these parameters were determined numerically. This was done by explicitly calculating values for α^c and γ^c as a function of α^d and γ^d for each particle, and comparing with the measured values. For γ^d, a range from 0 to π radians was used, with a resolution equivalent to 0.05 degrees. For α^d, a range from 0.00 to 0.20 was chosen based on the typical measured values, with a resolution of 2×10^{-5}. For particles where the best values were found to be close to the limit of this range in α^d, a larger range from 0 to 0.60 was then calculated at the same resolution.

When calculating values for α^c and γ^c, Eq. 14 has both positive and negative solutions. We only took the positive solution since this corresponds to the measured α, however, Eq. 15 also has multiple solutions, corresponding to either the positive or negative α^c. To check whether the calculated value of γ^c is the correct solution for positive α^c, we compared the results of Eq. 13 with the results of Eq. 5 for $\sigma = 1$ and $\gamma_p = 0$. If the calculated γ^c corresponded to the negative α^c values, the two equations would disagree, and γ^c was changed by $\pi/2$ to chose the correct solution. The values for α^d and γ^d were then identified as the minima of the absolute difference between the measured and calculated complex values of $\alpha \exp(2i\gamma)$, an example of which for a single particle is shown in Fig. S4.

Finally the particles were thresholded according to the noise criteria discussed in the

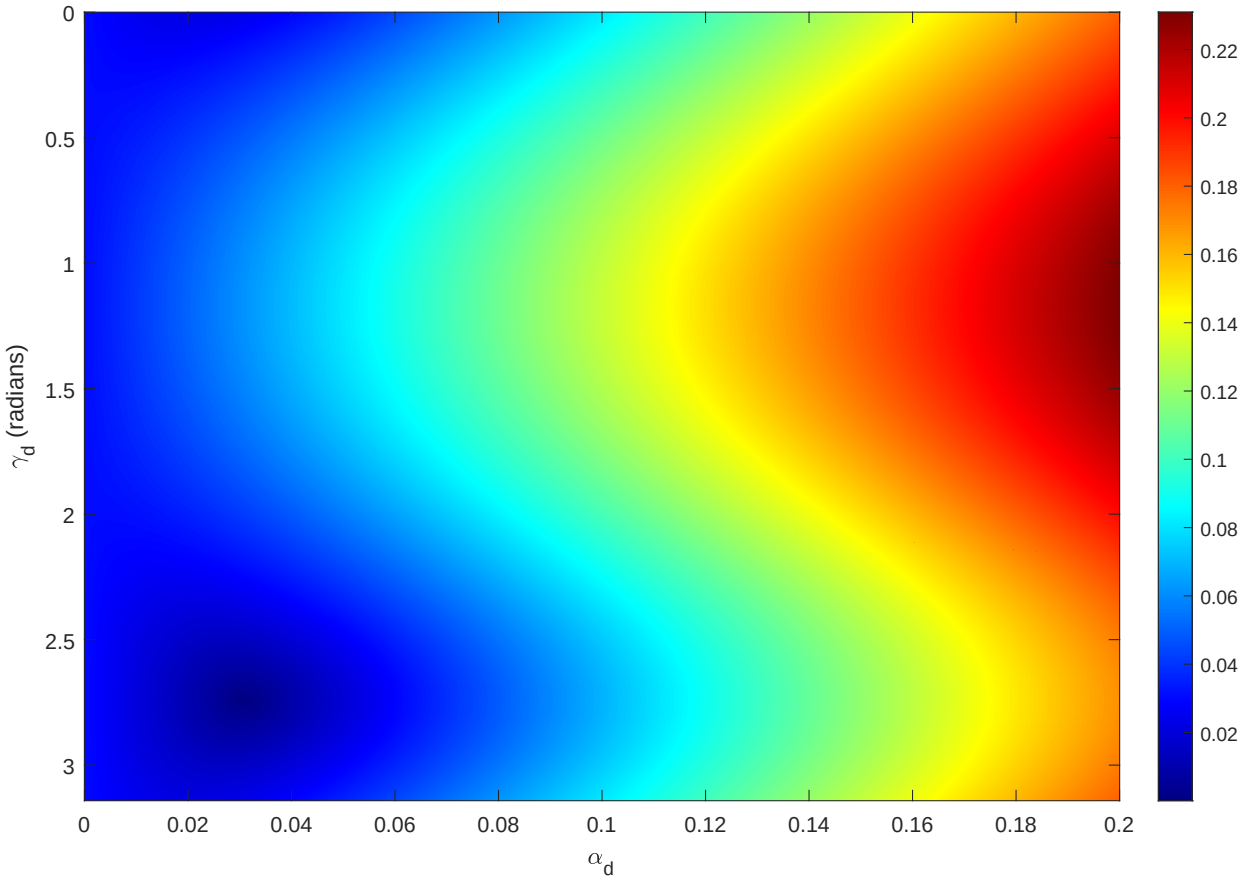

FIG. S4. An example of the RMS error between the calculated and measured complex parameter, $\alpha \exp(2i\gamma)$, for a selected sepia particle, plotted as a function of α^{d} and γ^{d}.

paper. The limits were chosen to be such as to result in z^{d} not significantly affected by measurement noise, leaving particles of larger size. To investigate if the results are robust with respect to the noise threshold chosen, we show below a repeat analysis with a significantly lower noise threshold for α, taking any particles with $\alpha^{\mathrm{c}}_{\Lambda} > 0.05$ for at least one wavelength. The lower threshold results in more particles being included in the analysis for each type of NP (25% of the total particles for L-DOPA, 17% for PDA, and 33% for sepia). The results of this analysis are shown in Fig. S5. As before, a Ripley's K-test was applied to the data, and the distribution of relative angles γ^{Δ} were again found to not be random.

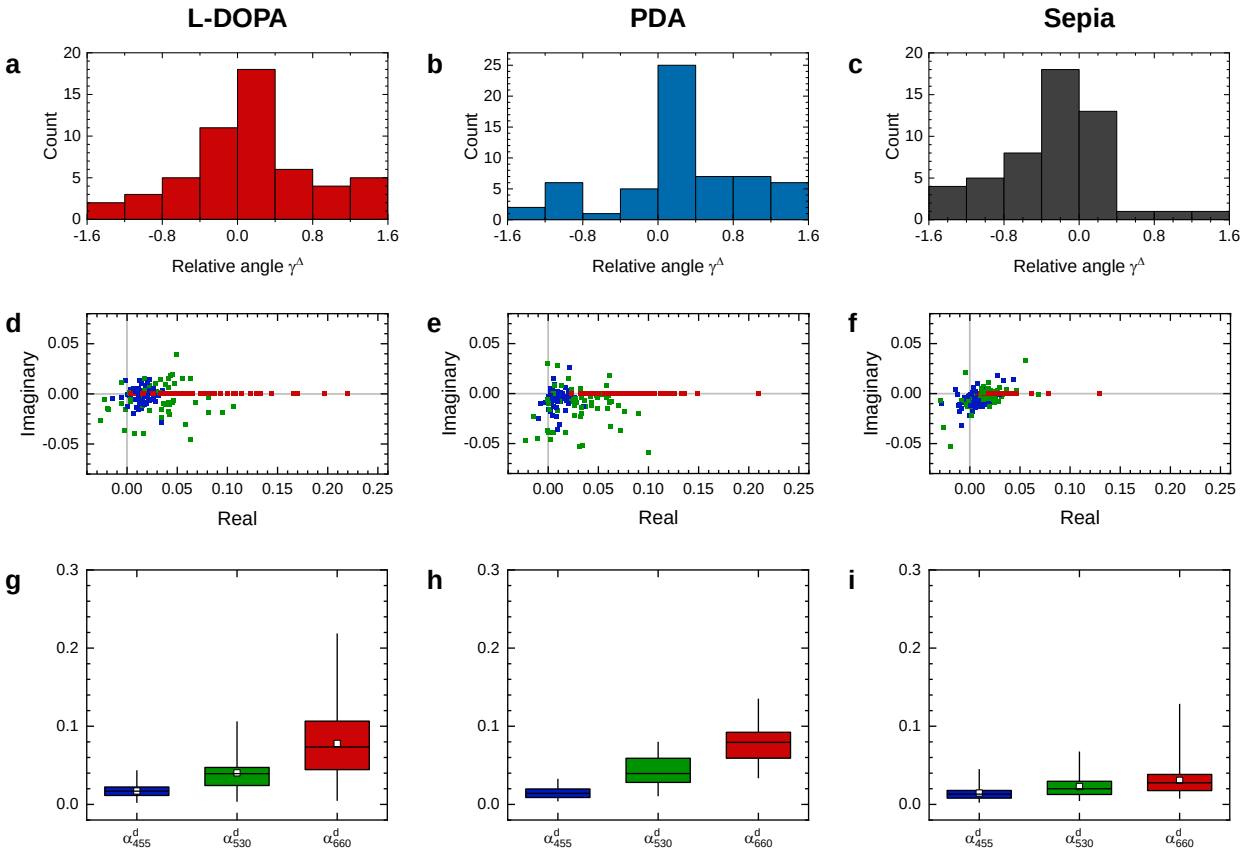

FIG. S5. Dichroism results as in Fig. 4, but using a lower noise threshold resulting in more particles analysed (see text). a-c) Histograms of γ^{Δ}, the relative angle of the change of dichroism from 455 nm to 530 nm and 455 nm to 660 nm, for the L-DOPA (a), PDA (b), and sepia (c) NPs. d-f) Dichroism in complex representation $z^{\mathrm{d}}_{\Lambda}\exp(-i\gamma^{\mathrm{d}}_{660})$, at 455 nm (blue), 530 nm (green), and 660 nm (red) for the L-DOPA (d), PDA (e), and sepia (f) NPs. g-i) The distribution of $\alpha^{\mathrm{d}}_{\Lambda}$ at each wavelength for L-DOPA (g), PDA (h), and sepia (i) NPs. The coloured boxes represent the interquartile range, with the horizontal line representing the median, and the white squares the mean. The vertical lines extend between minimum and maximum.

[1] Yuran Huang, Yiwen Li, Ziying Hu, Xiujun Yue, Maria T. Proetto, Ying Jones, and Nathan C. Gianneschi. Mimicking melanosomes: Polydopamine nanoparticles as artificial microparasols. *ACS Cent. Sci.*, 3(6):564–569, 2017. doi:10.1021/acscentsci.6b00230.

[2] Kuk-Youn Ju, Martin C. Fischer, and Warren S. Warren. Understanding the role of aggregation in the broad absorption bands of eumelanin. *ACS Nano*, 12(12):12050–12061, 2018. doi: 10.1021/acsnano.8b04905.

[3] Samuel Hamilton, David Regan, Lukas Payne, Wolfgang Langbein, and Paola Borri. Sizing individual dielectric nanoparticles with quantitative differential interference contrast microscopy. *Analyst*, 147:1567–1580, 2022. doi:10.1039/D1AN02009A.